Journal of Materials Chemistry B

ROYAL SOCIETY OF CHEMISTRY

PAPER

View Article Online
View Journal | View Issue

Cite this: J. Mater. Chem. B, 2023, 11, 6612

Bioimaging of glutathione variation for early diagnosis of hepatocellular carcinoma using a liver-targeting ratiometric near-infrared fluorescent probe†

Xiaoyue Han,‡[a] Yanlong Xing,‡*[bc] Xinyu Song,[d] Kun Dou,[bc] Fabiao Yu *[bc] and Lingxin Chen *[a]

Received 20th April 2023,
Accepted 21st May 2023

DOI: 10.1039/d3tb00893b

rsc.li/materials-b

Reliable biomarkers are crucial for early diagnosis of diseases and precise therapy. Biological thiols (represented by glutathione, GSH) play vital roles in the antioxidant defense system for maintaining intracellular redox homeostasis in organisms. However, the aberrant variation in the cellular concentration of GSH correlates with diverse diseases including cancer. Here, a ratiometric near-infrared fluorescent probe **CyO-Disu** is constructed for the specific sensing of GSH variation in live cells and mice models of hepatic carcinoma (HCC). **CyO-Disu** features three key elements, a response moiety of bis(2-hydroxyethyl) disulfide, a near-infrared fluorescence signal transducer of heptamethine ketone cyanine, and a targeting moiety of D-galactose. By virtue of its liver-targeting capability, **CyO-Disu** was utilized for evaluating GSH fluctuations in primary and metastatic hepatoma living cells. To evaluate the efficacy of **CyO-Disu** *in vivo*, orthotopic HCC and pulmonary metastatic hepatoma mice models were employed for GSH imaging using two-dimensional and three-dimensional fluorescence molecular tomographic imaging systems. The bioimaging results offered direct evidence that GSH displayed varied concentrations during the progression of HCC. Therefore, the as-synthesized probe **CyO-Disu** could serve as a potential powerful tool for the early diagnosis and precise treatment of HCC using GSH as a reliable biomarker.

1. Introduction

The cellular redox state is of critical importance in various physiological and pathological events, including controlling of the cell cycle, regulation of programmed cell death, and activation of cytokine and growth factor gene expression.[1] The disturbance of redox homeostasis results in a variety of pathological processes ranging from neurodegenerative disease, diabetes mellitus, ageing and cancer.[2,3] In organisms, antioxidant defense systems composed of antioxidant enzymes and small molecular antioxidants account for removing the excessive reactive oxygen species (ROS) and maintaining the intracellular redox hemostasis.[4] As the most abundant low-molecular-weight non-protein biothiols, glutathione (GSH) exerts its function by adjusting the reduced and oxidized forms through a mercapto-disulfide exchanging mechanism.[5] GSH has an intracellular concentration of 1 to 10 mM. However, the aberrant concentration ratio between the mercapto-disulfide redox status is highly related to the progression of varieties of diseases such as cancer. Among the various cancer types, hepatocellular carcinoma (HCC) is the malignant tumor whose mortality of cancer ranks the second highest globally.[6] The proliferation, motility, apoptosis, and senescence of HCC cells are closely related to the intracellular redox metabolism changes. Hence, it is imperative to detect the GSH level changes for understanding the redox state in the development of HCC by utilizing a selective and sensitive chemical tool.

To date, analytical techniques detecting GSH include the enzymatic recycling method, high-performance liquid chromatography,

[a] CAS Key Laboratory of Coastal Environmental Processes and Ecological Remediation, Yantai Institute of Coastal Zone Research, Chinese Academy of Sciences, Yantai 264003, China. E-mail: lxchen@yic.ac.cn
[b] Key Laboratory of Hainan Trauma and Disaster Rescue, The First Affiliated Hospital of Hainan Medical University, Hainan Medical University, Haikou 571199, China. E-mail: xingyanlong@hainmc.edu.cn, yufabiao@hainmc.edu.cn
[c] Engineering Research Center for Hainan Bio-Smart Materials and Bio-Medical Devices, Key Laboratory of Hainan Functional Materials and Molecular Imaging, Key Laboratory of Emergency and Trauma, Ministry of Education, College of Emergency and Trauma, Hainan Medical University, Haikou 571199, China
[d] State Key Laboratory of Respiratory Disease, Guangzhou Institute of Respiratory Health, National Clinical Research Center for Respiratory Disease, The First Affiliated Hospital of Guangzhou Medicine University, Guangzhou 510120, China

† Electronic supplementary information (ESI) available. See DOI: https://doi.org/10.1039/d3tb00893b

‡ F X. Han and Y. Xing contributed equally.

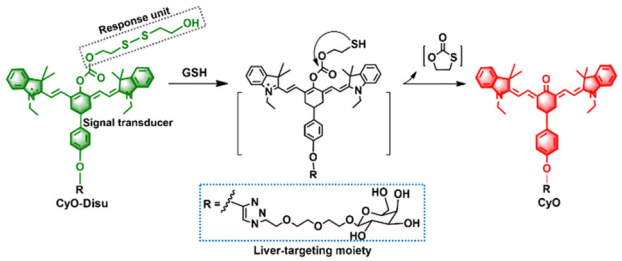

Scheme 1 The molecular structure of **CyO-Disu** and the proposed reaction mechanism against GSH.

capillary electrophoresis, *etc.*[7,8] Nevertheless, these approaches suffer from complex sample pre-treatment and difficulty in visualization, which make them unsuitable for real-time and *in situ* GSH measurement in live cells and *in vivo*. Due to the advantages of excellent spectral characteristics, high spatiotemporal resolution, high sensitivity and selectivity, various small molecular fluorescent probes have been constructed for different biomolecules,[9–15] including GSH,[16–19] based on the strong nucleophilicity and reducibility properties of the mercapto unit.[20,21] However, an efficient imaging tool being capable of dynamically and *in situ* evaluating GSH fluctuation in early and advanced stages of mice HCC models has not been reported yet.

Herein, we propose a new near-infrared (NIR) fluorescent probe **CyO-Disu** to evaluate GSH by ratiometric signal in live cell lines and mice models (Scheme 1). **CyO-Disu** consisted of three components: a ketone cyanine fluorophore (Keto-Cy) as the NIR fluorescence signal transducer, bis(2-hydroxyethyl) disulfide as the response unit for GSH, and D-galactose as the moiety to target liver. The spectral properties of **CyO-Disu** indicate that this probe could rapidly respond to GSH in around 5 min, which is beneficial for real-time imaging in live cells and mice. Various liver cells and liver cancer cells were independently imaged with **CyO-Disu** to evaluate the probe's capability in measuring GSH changes in cells. Furthermore, the fluctuation of the endogenous GSH level during the process from orthotopic hepatoma to pulmonary metastatic hepatoma was successfully tested with **CyO-Disu** using two-dimensional (2D) and three-dimensional (3D) fluorescence molecular tomographic (FMT) imaging technique. To the best of our knowledge, **CyO-Disu** is the first fluorescent probe which evaluates the concentration variation of GSH in different stages of mice HCC models.

2. Experimental

Synthesis and characterization of CyO-Disu

The synthesis of **CyO-Disu** is based on a previously reported work.[22] Briefly, CyO-R′ (11.3 mg, 0.1 mmol) and triphosgene (9.0 mg, 0.3 mmol) were dissolved in anhydrous CH_2Cl_2 (50 mL) under Ar protection. After suspending the mixture at 0 °C, *N*,*N*-diisopropylethyl-amine (DIPEA) (1 mL) was added. Then the mixture was stirred for half an hour, until the color changed from red to green. Upon removing the solvent under vacuum, the crude product was dissolved in anhydrous CH_2Cl_2 (50 mL). Afterwards, 1 mL of DIPEA, 20 mg of 4-dimethylaminopyridine (DMAP), and 2,2′-dithiodiethanol (30.0 mg, 0.2 mmol, in 2 mL CH_2Cl_2) were subsequently added to the above solution with stirring at 25 °C. Thin layer chromatography was used to monitor the reaction. The resultant solid was separated and applied to silica gel chromatography (200–300 mesh) for purification using a gradient eluent (CH_2Cl_2–CH_3OH, 1 to 85/15 v/v). After the solvent removing step under vacuum, the residue was dissolved in CH_2Cl_2. After filtration and evaporation, a green solid was generated (113.8 mg, yield 87%), which was then dissolved in 5 mL of methanol (1.2 mL of 0.5 M potassium carbonate solution). The reaction was further kept at 25 °C for 1 h under stirring. Following neutralization by adding 5% hydrochloric acid, the mixture was treated with CH_2Cl_2 (3 times, 50 mL each) to separate. Then anhydrous Na_2SO_4 was utilized to dry the organic layer. After concentration under vacuum, the obtained solid was purified using column chromatography (200–300 mesh) with the eluent of CH_2Cl_2–CH_3OH (8/1, v/v) to obtain **CyO-Disu** as a green product (10.3 mg, 15%). The characterization is as follows: ^{1}H NMR (500 MHz, $CDCl_3$-D_1) δ (ppm): 8.63–8.61 (d, J = 7.6, 1.0 Hz, 1H), 8.45–8.39 (m, 1H), 7.92–7.86 (m, 1H), 7.78–7.73 (m, 1H), 7.59–7.58 (m, 1H), 7.39–7.37 (d, J = 7.6, 1.3 Hz, 1H), 7.30–7.28 (m, 2H), 7.19–7.18 (d, J = 7.6, 1.3 Hz, 1H), 7.08–7.03(m, 3H), 6.83–6.81(d, J = 11.6, 6.5 Hz, 1H), 5.50–5.46 (q, 1H), 5.42–5.39 (d, J = 12.1, 6.5 Hz, 1H), 5.26–5.17 (m, 3H), 5.06–5.01 (m, 1H), 4.64–4.54 (m, 3H), 4.18–4.13 (q, 2H), 3.94–3.92 (m, 4H), 3.81–3.75 (m, 4H), 3.66–3.60 (m, 12H), 2.56–2.50 (m, 2H), 2.26–2.23 (m, 2H), 2.06 (m, 9H), 1.69–1.65 (t, 3H), 1.32–1.27 (m, 12H), 0.91–0.88 (t, 6H). ^{13}C NMR (125 MHz, $CDCl_3$-D_1) δ (ppm): 170.23, 169.97, 150.45, 143.70, 136.64, 133.21, 129.84, 129.58, 127.99, 127.81, 124.24, 122.17, 121.29, 115.67, 114.90, 110.21, 107.63, 101.20, 98.32, 92.50, 70.73, 70.72, 70.44, 70.08, 69.29, 69.04, 68.68, 66.91, 61.88, 61.08, 53.30, 50.22, 50.21, 47.45, 37.49, 35.79, 34.06, 31.77, 31.75, 29.54, 29.50, 29.20, 28.97, 28.54, 27.07, 24.20, 20.66, 20.53, 20.45, 13.97, 11.23. LC-MS (ESI$^+$): m/z $C_{60}H_{78}N_5O_{13}S_2^+$ calcd 1140.5032, found [M^+] 1140.5033.

2D and 3D imaging of mice

A Fluoroscopic Navigator 360I System was employed to 2D *ex vivo* and *in vivo* fluorescence imaging. PerkinElmer IVIS Spectrum Series was selected for 3D fluorescence molecular tomographic imaging. The choice of suitable excitation and emission wavelengths is illustrated in Fig. 4 and 5. Mice were anaesthetized with isoflurane before administering fluorescent probes and throughout the imaging procedure.

3. Results and discussion

Design strategy of the probe CyO-Disu

Intracellular low-molecular-weight reduced thiols such as GSH, Cys, and Hcy are essential for maintaining cellular redox homeostasis. Therefore, evaluating the content of these biothiols in HCC cells is imperative. In this case, two key points need to be

taken into consideration. One is the different nucleophilicity and reducibility of these biothiols (the pK_a value of GSH is 8.75, with 8.29 for Cys, and 10.0 for Hcy),[23] and the other is the varied intracellular concentration (GSH is in 1 to 10 mM level, while Cys and Hcy are of micromolar levels).[24,25] Inspired by the thiol-disulfide exchange reaction which functions in cells to regulate the cellular redox homeostasis,[26] the disulfide was adopted as the thiols response unit.[27,28] To obtain better thermodynamics and reaction kinetics, a reactive ester bridge was chosen.[29] The absorption coefficients of heme, water, lipids, and the major absorbers are higher in the visible and infrared light regions but lower in the NIR region around 650–900 nm.[30–33] Therefore, a cyanine fluorophore bearing ketone (Keto-Cy) was selected as the NIR fluorescence signal transducer. To achieve the liver-targeting capability, the probe introduced the galactose terminated ligand which could be selectively identified by the asialoglycoprotein receptor (ASGP-R), due to its specific expression on the plasma membrane of mammalian liver cells. The procedure to synthesize the probe **CyO-Disu** is depicted in Scheme S1 (ESI†).

Ratiometric fluorescence analysis is based on the ratio of signal fluctuations, which can minimize the interferences from the uneven distribution of probe in cells and instrument variables.[29,34] Herein, the developed probe **CyO-Disu** can achieve ratiometric imaging in live cells and mice, which is critical to obtain reliable information at the intracellular thiol level. As showcased in Scheme 1, the disulfide of the probe could be effectively reduced by thiols (represented with GSH) to expose a thiol group. Upon the nucleophilic addition of the thiol group, the fluorophore was released to generate new emission spectra for ratiometric analysis with the probe.

Spectral characteristics and selectivity of the probe CyO-Disu

To understand the UV/vis and fluorescence spectral properties of probe **CyO-Disu** towards thiols, GSH was selected as the representative. Upon the addition of 0–10 mM of GSH in HEPES buffering solution (10 mM, pH 7.4, Fig. S1, ESI†) at 37 °C, the absorption peak shifted from 788 nm (ε_{788} nm = 1.89 × 10^4 M^{-1} cm^{-1}) to 528 nm (ε_{528} nm = 4.15 × 10^4 M^{-1} cm^{-1}), with the color of the solution changing from green to red (Fig. 1a). Moreover, the fluorescence maximum emission wavelength varied from 783 nm (Φ_{783nm} = 0.13) to 613 nm (Φ_{613nm} = 0.06) (Fig. 1b and c). The fluorescence intensity ratio (F_{613nm}/F_{783nm}) exhibited a positive correlation with GSH concentration (Fig. 1d). In addition, a linear relationship between lg(Ratio) and the concentration of GSH within 0–10 mM (Fig. 1d, inset) is illustrated. The regression equation was expressed as lg(Ratio) = 0.173 [GSH] mM − 0.45, with an r value of 0.9935. The actual limit of detection in experiment was measured to be 2 μM while the theoretical detection limit was 65 nM (3 σ/k). Herein, σ represents the standard deviation, while k is the slope of the regression equation.

Afterwards, the selectivity of the probe **CyO-Disu** to GSH was tested. All the detection lasted 5 min. As depicted in Fig. 1e, upon exposure to various specimens in HEPES (10 mM, pH 7.4), **CyO-Disu** displayed a strong ratio fluorescence signal towards

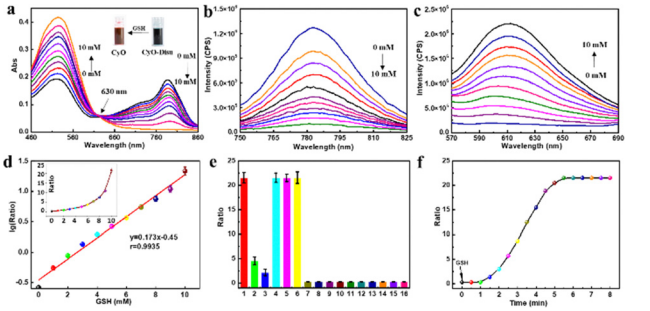

Fig. 1 Spectral characteristics and selectivity of **CyO-Disu**. (a) Absorption spectra, (b) emission spectra (excitation at 710 nm) and (c) emission spectra (excitation at 535 nm) spectra of **CyO-Disu** to GSH. **CyO-Disu** (10 μM) was incubated with GSH (0–10 mM) at 37 °C in HEPES (10 mM, pH 7.4). The spectra were measured after 6 min. (d) Linear correlation between lg(F_{613nm}/F_{783nm}) and GSH concentration (0 – 10 mM). Inset: change of the intensity ratio (F_{613nm}/F_{783nm}) of **CyO-Disu** (10 μM) as a function of GSH (0–10 mM). (e) Fluorescence ratio (F_{613nm}/F_{783nm}) response of **CyO-Disu** (10 μM) to various thiols and other non-thiol amino acids at 37 °C in HEPES (10 mM, pH 7.4). 1, 10 mM GSH; 2, 200 μM Cys; 3, 10 μM Hcy; 4, 10 mM dithiothreitol (DTT); 5, 10 mM 2-mercaptoethanol (2-ME); 6, 2-aminoethanethiol (2-AET); 7, 10 μM Trx; 8, 10 mM Glu; 9, 10 mM Pro; 10, 10 mM Ala; 11, 10 mM Phe; 12, 10 mM Ser; 13, 10 mM Val; 14, 10 mM Arg; 15, 10 mM His; and 16, blank. The spectra were recorded after 5 min. (f) Time-dependent fluorescence ratio F_{613nm}/F_{783nm} of **CyO-Disu** (10 μM) to GSH (10 mM) in a time range of 0–8 min. GSH was introduced into the reaction at initiation in HEPES (10 mM, pH 7.4). Measurement was performed for 8 min. F_{613nm}: λ_{ex} = 535 nm, λ_{em} = 613 nm; F_{783nm}: λ_{ex} = 710 nm, λ_{em} = 783 nm. All the measurements have been repeated three times, and the mean (± s.d.) data are displayed.

GSH. Micromolar level of Cys and Hcy also exhibited a fluorescence signal, while not competitive to that of GSH. With the purpose of verifying the reaction mechanism of **CyO-Disu** towards the thiol group, thiols of chemical origin including 2-aminoethanethiol (2-AET), 2-mercaptoethanol (2-ME) and dithiothreitol (DTT) were applied to the detection system. The high fluorescence signal evidently demonstrated the response mechanism of the developed probe towards thiols upon the cleavage of the disulfide bond. In addition, owning to steric hindrance, **CyO-Disu** displayed neglectable response towards thioredoxin reductases (Trx). Other non-thiol amino acids (Glu, Pro, Ala, Phe, Ser, Val, Arg and His), ROS, reactive nitrogen species (RNS), metal ions and anions merely induced ignorable signal (Fig. 1e and Fig. S2, ESI†). Therefore, the probe **CyO-Disu** can selectively detect GSH without interference from other biologically relevant analytes. Furthermore, the reaction kinetics of **CyO-Disu** to GSH was carried out. The ratio-fluorescence signal response was recorded from 0 to 8 min upon adding GSH (10 mM). As displayed in Fig. 1f and Fig. S3 (ESI†), the addition of GSH induced the ratio-fluorescence enhancement and reached a plateau after ∼5 min. The reaction kinetics results demonstrated that probe **CyO-Disu** could be utilized as an effective tool for the bioimaging of intracellular GSH in a real-time manner.

Fluorescence imaging of GSH in living cell models

Since probe **CyO-Disu** has been successfully employed for the selective and sensitive detection of GSH *in vitro*, it was further

harnessed to investigate the endogenous GSH concentration generation in different types of cells. In a first step, the cytotoxicity of **CyO-Disu** was assessed by MTT (3-[4,5-dimethylthiazol-2-yl]-2,5 diphenyl tetrazolium bromide) assays. Rat hepatoma cells (RH-35), rat liver cells (BRL 3A), human HCC cells (SMMC-7721) and human heptocyte cells (HL-7702) were chosen as cytotoxicity testing models. As illustrated in Fig. S4 (ESI†), the high cell viability results demonstrated the low cytotoxicity of **CyO-Disu** to living cells. Prior to imaging, 10 μM **CyO-Disu** was added to the tested cells for 5 min (37 °C, 95% humidified atmosphere with 5% CO_2). As displayed in Fig. 2a, the ratio of fluorescence signal exhibited increment in the time range of 0–5 min in the detected cells. Nevertheless, the four cell types exhibited distinguishable response resulting from the distinct GSH generation abilities. The mean ratio intensity was ranked as: RH-35 > SMMC-7721 > BRL 3A > HL-7702 (Fig. 2b), which is in accordance with the GSH concentration calculated using the equation in Fig. 1d and Fig. S5 (ESI†). The flow cytometry experiment was performed at 0 and 5 min, respectively. As depicted in Fig. 2c and d, the mean ratio intensities at 5 min were in the sequence of RH-35 > SMMC-7721 > BRL 3A > HL-7702, which was consistent with the confocal imaging results. Since Ki67 is a cellular marker for cell proliferation, Ki67 expression in the cells was further evaluated with the immunofluorescence analysis method by staining anti-Ki67 mAb (Alexa Fluor 647 Conjugate). As illustrated in Fig. 2e, the expression level of Ki67 in these cells was exhibited to be RH-35 > SMMC-7721 > BRL 3A > HL-7702, which presented a positive correlation with intracellular GSH concentration. Not only the contents of GSH but also the corresponding expression level of Ki67 were higher in hepatocellular carcinoma cells (RH-35 and SMMC-7721) than those in normal hepatocytes (BRL 3A and HL-7702), implying that probe **CyO-Disu** could be utilized as an effective tool to evaluate the endogenous GSH level and cell proliferation degree.

Fluorescence imaging of endogenous GSH changes

Based on the bioimaging of GSH in various live cells, we then tested the capability of **CyO-Disu** for sensing the fluctuation of intracellular GSH upon exogenous stimulation. Herein, RH-35 cells were employed and stimulated by various chemical regents. As displayed in Fig. 3a, the cells in the control group portrayed a high intensity ratio, suggesting abundant GSH in living cells.

After pretreatment with *N*-ethylmaleimide (NEM) (5 mM, 30 min), a thiol-blocking agent, the cells emitted neglectable fluorescence, due to complete depletion of cellular GSH by NEM. Buthionine sulphoximine (BSO) which can inhibit *gamma*-glutamylcysteine synthetase (γ-GCS) is capable of reducing the intracellular GSH concentration. The addition of BSO (1 mM, 2 h) to normal living cells displayed a faint ratio of fluorescence signal, suggesting the low intracellular GSH level. Upon treatment of cells with 100 μM GSH-MEE, an exogenous GSH supplement,[35] for 20 min, the increased high ratio fluorescence signal indicated the increment of the intracellular GSH level caused by GSH-MEE. *N*-Acetylcysteine (NAC) is a precursor of Cys.[36] The application of NAC (1 mM, 2 h) in living cells exhibited an increased ratio of fluorescence signal compared with the control group, attributing to the increased intracellular GSH concentration. Fig. 3b displayed the average ratio intensities of images in Fig. 3a, which also obviously proved the imaging output. Following this, flow cytometry analysis was performed to observe fluorescence intensity changes caused by GSH fluctuations (Fig. 3c). These results were in accordance with those obtained from the confocal fluorescence images (Fig. 3b and d). All the above measurements demonstrated that the probe **CyO-Disu** was capable of imaging the endogenous GSH concentration changes in the living cells.

Visualization of GSH in the early stage of mouse HCC

Encouraged by the successful application of **CyO-Disu** in detecting GSH level fluctuation in living cells, we further

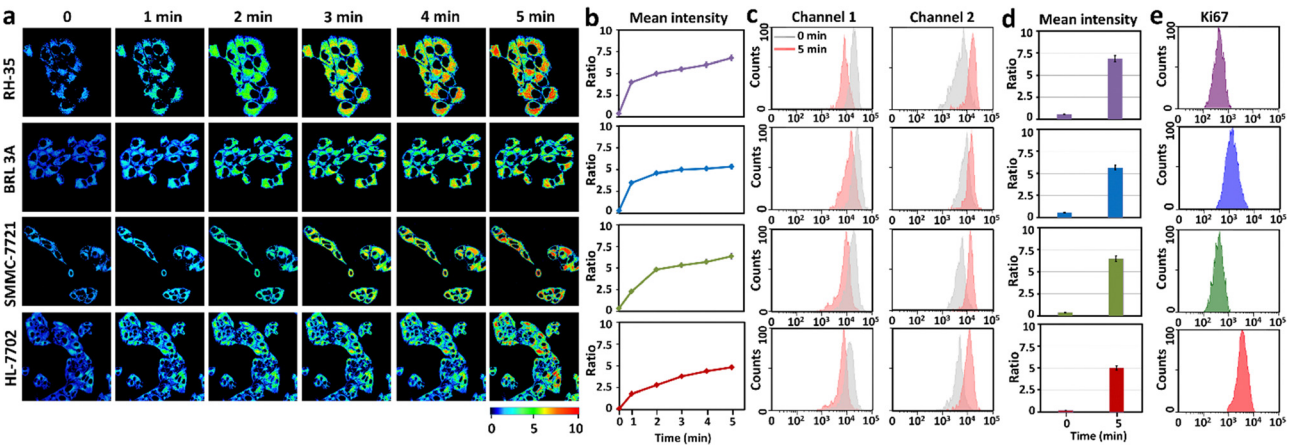

Fig. 2 Fluorescence imaging of the generation of endogenous GSH by probe **CyO-Disu** in living RH-35, BRL 3A, SMMC-7721, and HL-7702 cells. (a) Pseudocolored ratiometric images of endogenous GSH generation at different times: 0, 1, 2, 3, 4, and 5 min. (b) Average ratio intensities of **CyO-Disu** against time. (c) Flow cytometry results and (d) the corresponding mean ratio intensity at 0 and 5 min. (e) Histograms of Ki67 expression immunofluorescence response. The experiments were repeated three times, with the data shown as mean (± s.d.). The differences between 0 min and any other groups were analyzed *via* one-way ANOVA and Bonferroni *post hoc* test. The variance between the detected groups was analyzed *via* Student's *t*-test. * $P < 0.05$, ** $P < 0.01$ and *** $P < 0.001$ was statistically significant.

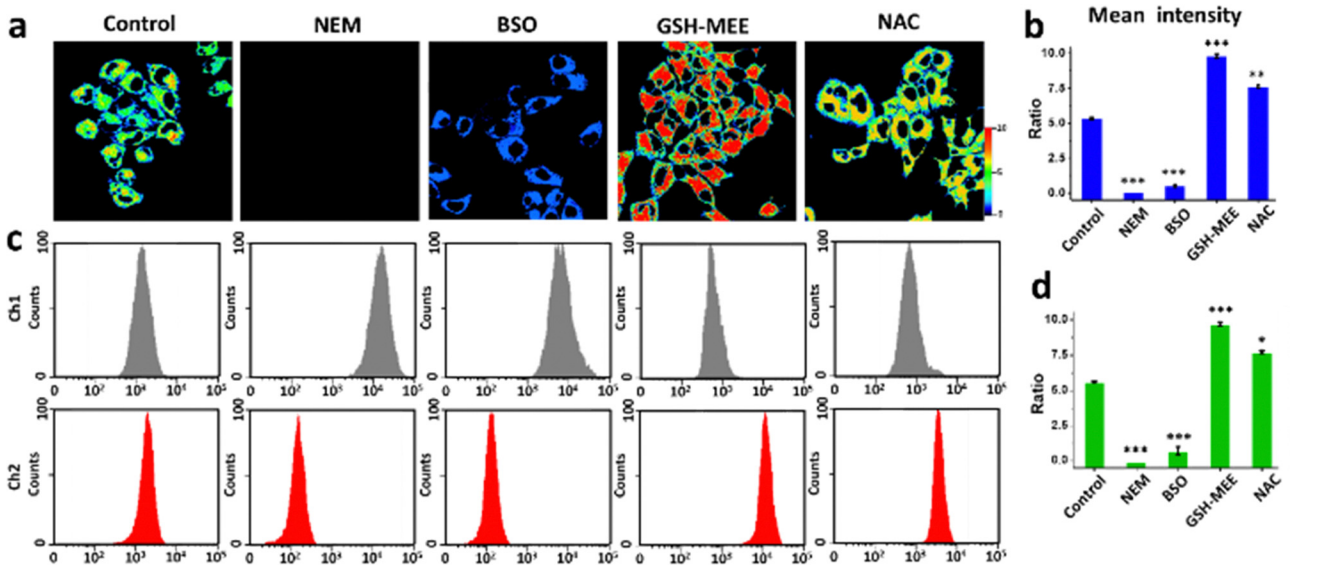

Fig. 3 (a) Pseudocolored ratiometric images of intracellular endogenous thiol concentration fluctuations in living RH-35 cells. (b) Average ratio intensities of images in (a) (number of cells, n = 7). (c) Flow cytometry analysis and (d) relevant mean ratio intensities. The measurement was repeated three times, with the data displayed as mean (±s.d.). The differences between the control group and any other groups were analyzed *via* one-way ANOVA followed by Bonferroni *post hoc* test. The differences between the two groups were analyzed *via* Student's t-test. * $P < 0.05$, ** $P < 0.01$ and *** $P < 0.001$ was statistically significant.

intended to examine the bioimaging capability of **CyO-Disu** in the early stage of mouse HCC. The galactose moiety in the probe **CyO-Disu** has been verified to be able to target in the liver.[37] Orthotopic hepatoma mice models were established by inoculating H22 cells in the capsule of the left hepatic lobe for 7, 14, 21 and 28 days. Both the 2D fluorescence imaging and 3D FMT imaging shown in Fig. 4a–c were obtained from two fluorescence collection windows: channel 1 (excitation filter: 730 nm, emission window: 780–800 nm) and channel 2 (excitation filter: 600 nm, emission window: 680–730 nm). The ratios representing the mean number of photons in Ch 2 *vs.* Ch 1 of Fig. 4a–c are displayed in Fig. 4e–g. As exhibited in Fig. 4a and e, the 2D *in vivo* ratio signal after 7 days of administration was higher than that of the control group (0 day). This is due to the increased GSH generation because of active proliferation and rapid expansion at the early stage of tumor development.[38] However, the 2D *in vivo* ratio signal decreased after 14 days, indicating the decreased GSH level from 14 days to 28 days. This result could be attributed to the overproduction of ROS with the progression of tumor.[39] Fig. 4a depicts the *ex vivo* imaging of GSH in the isolated organs (heart, liver, spleen, lungs, and kidneys) from the mice after sacrifice. As showcased in Fig. 4b and f, the probe **CyO-Disu** exhibited selective liver-targeting ability. In addition, the ratio signal in liver increased at 7 days and decreased after 14 days, which was consistent with the results shown in Fig. 4a and e.

To investigate the GSH distribution in deep hepatoma tissue, we further performed 3D FMT imaging according to the accurate reconstruction of the fluorescence dissemination *in vivo*.[40] The 3D FMT fluorescence imaging of the mice bearing orthotopic hepatoma was rebuilt *via* diffuse tomographic algorithms. The GSH localization in hepatoma was also apparently displayed with different views of coronal, sagittal, and transverse sides (Fig. 4c). The 3D reconstruction of *in vivo* fluorescence imaging results also demonstrated that the GSH level increased from 0 day to 7 days and then decreased from 14 days to 28 days (Fig. 4g). The successful establishment of orthotopic hepatoma mouse models was proved by H&E staining of liver tissue (Fig. S9, ESI†) and the expression of cell proliferation protein marker Ki67 by immunofluorescence (Fig. 4d and h). The increased expression of Ki67 from 0 day to 28 days obviously validated the proliferation and rapid growth of the tumor cells in orthotopic hepatoma mice. All the above results revealed that the GSH level change in the early stage of mouse HCC underwent an increase and decrease process, which might be employed for the evaluation of tumor development and therapy.

Evaluation of GSH in the advanced stage of mouse HCC

Metastasis of orthotopic lesion to distant sites through either blood circulatory system or lymphatic system frequently happens at the advanced stage of cancer and accounts for around 90% of cancer death. The metastatic cancer cells are homologous with the primary hepatoma cells and contain a similar GSH level. Therefore, the progression of liver cancer could be recognized by the probe **CyO-Disu**, according to the fluorescence imaging of liver and other organs. Lung is the most common site of extrahepatic HCC metastases.[41] The accurate location of metastatic lesion would assist further precision therapy.

To verify whether the probe could track the metastasis of hepatoma, we established the pulmonary metastatic HCC mouse model.[42,43] The macroscopy photos of the primary and metastasis tumor lesions on 35 days, 42 days, and 49 days after

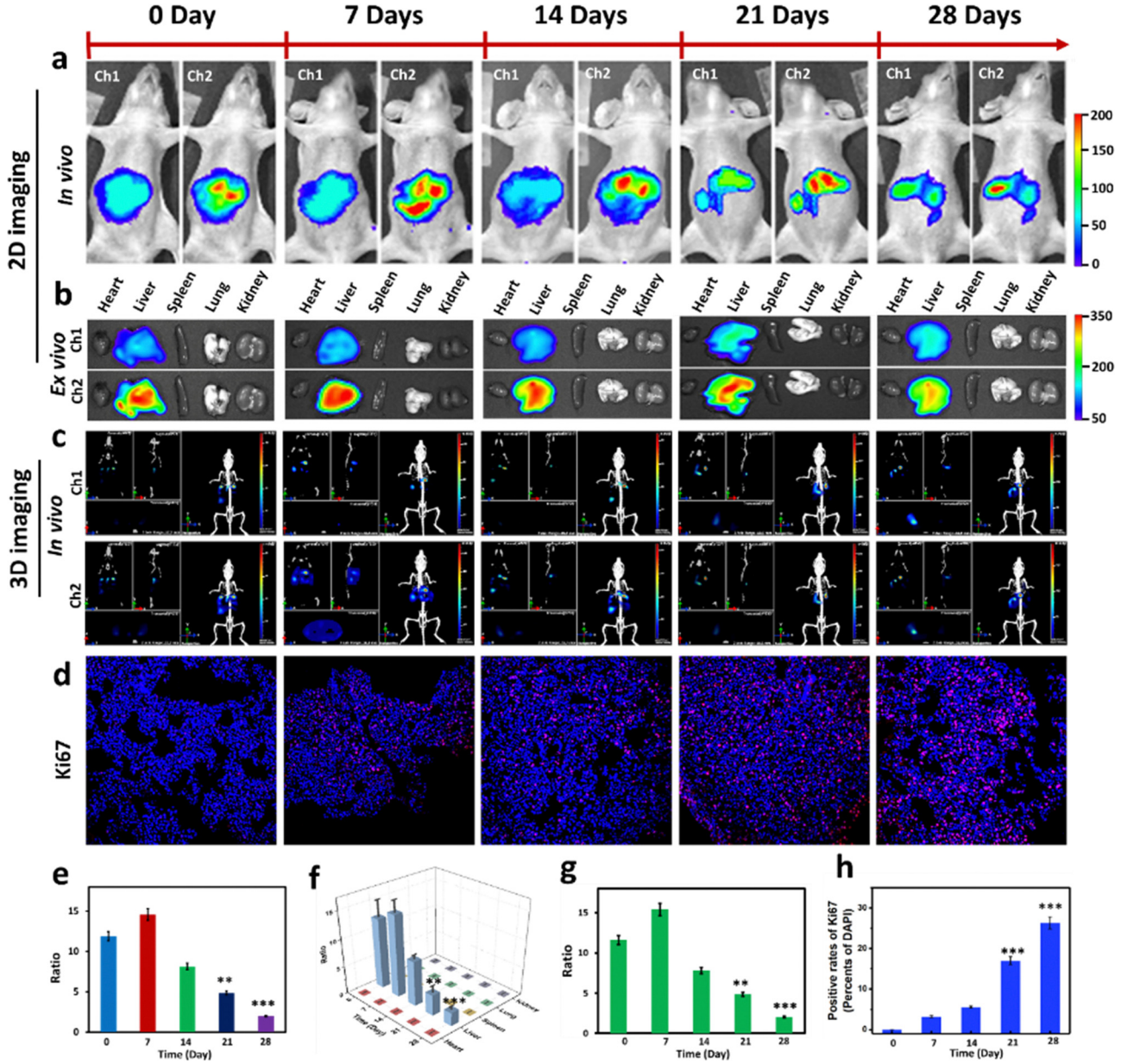

Fig. 4 Visualization of GSH in the orthotopic mouse HCC model. (a) 2D bioimaging of GSH in mice after tail vein injection of **CyO-Disu** (10 μM, 200 μL, in in DMSO-saline, 1/99, v/v) for 15 min (n = 3 each group). (b) 2D *ex vivo* imaging of GSH in isolated organs (heart, liver, spleen, lungs, and kidneys) sacrificed from (a). (c) 3D reconstruction of FMT imaging of GSH from coronal, sagittal, and transverse views. **CyO-Disu** (10 μM, 200 μL in DMSO-saline, 1/99, v/v) was administered *via* tail vein for 15 min before bioimaging (n = 3 per group). (d) Expression of proliferation protein marker Ki67 with anti-Ki67 mAb (Alexa Fluor 647 conjugate, $\lambda_{ex}/\lambda_{em}$ =635 nm, 670–770 nm, red channel) and nucleus (DAPI, $\lambda_{ex}/\lambda_{em}$ = 405 nm, 410–490 nm, blue channel) in tumor sections. Scale bar: 50 μm. (e) Average ratio of the intensity in (a). (f) Mean ratio intensity values of the organs in (b). (g) Ratio value of fluorescence intensity in (c). (h) The statistical analysis of the data from (d). The measurement was repeated three times, with the data displayed as mean (± s.d.). The differences between the control group (0 day) and any other groups were analyzed *via* one-way ANOVA followed by Bonferroni *post hoc* test. The variation between different groups was analyzed *via* Student's t-test. * $P < 0.05$, ** $P < 0.01$ and *** $P < 0.001$ was statistically significant.

administration are displayed in Fig. 5a, in which the white arrows pointed out the typical tumor nodules. The H&E staining results (Fig. 5b) also demonstrated the successful establishment of a pulmonary metastatic HCC mouse model. Thanks to the galactose terminated ligand on the probe **CyO-Disu**, the ASGP-R especially expressed on the plasma membrane of hepatoma cells would be recognized by the probe, which made the fluorescence imaging of pulmonary metastatic HCC cells possible. Following, we performed 3D FMT imaging of GSH from views of coronal, sagittal, and transverse sides in the pulmonary metastatic HCC mice after 35-, 42- and 49-days' administration of the probe. As shown in Fig. 5c, the fluorescence in Ch 1 gathered both in the thoracic and superior abdominal cavities. To further verify the locating organs of

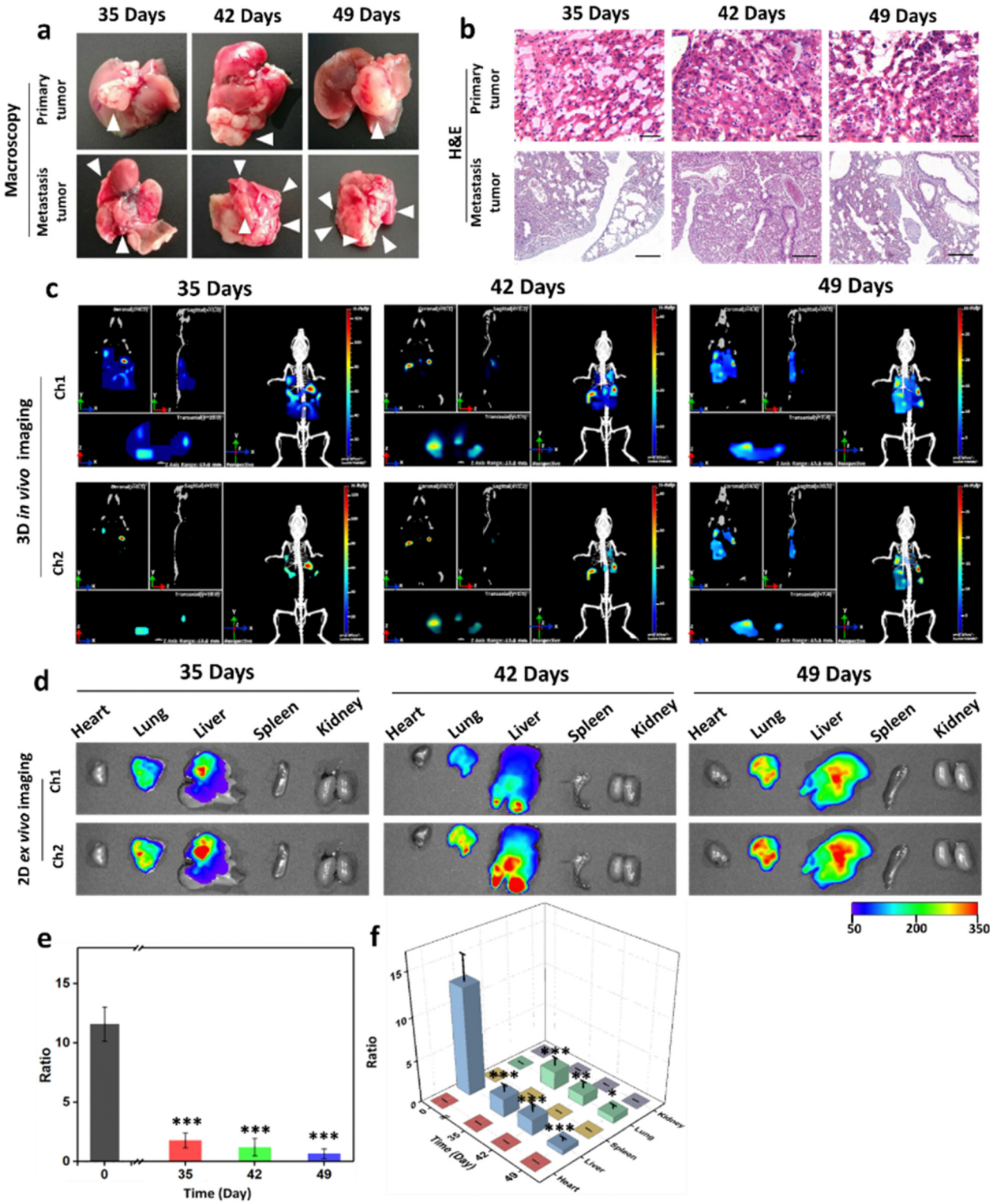

Fig. 5 Evaluation of GSH in pulmonary metastatic HCC mice models. (a) Macroscopic appearance of the primary tumor and metastasis tumor tissues. (b) H&E staining of the primary tumor (scale bar: 50 μm) and metastasis tumor tissues (scale bar: 200 μm). (c) 3D reconstruction of *in vivo* imaging of GSH from coronal, sagittal, and transverse views, as well as the 3D image after tail vein injection of **CyO-Disu** (10 μM, 200 μL, in DMSO-saline, 1/99, v/v) for 15 min. (d) 2D bioimaging of GSH in isolated organs (heart, liver, spleen, lungs, and kidneys) from the mice in (c). (e) Average ratio of the intensity values in (c). (f) Mean ratio intensity values of relevant organs in (d). The measurement was repeated three times, with the data displayed as mean (± s.d.). The differences between the 0-day (control) group and any other groups were analyzed *via* one-way ANOVA followed by Bonferroni *post hoc* test. The variation between the different groups was analyzed *via* Student's *t*-test. * $P < 0.05$, ** $P < 0.01$ and *** $P < 0.001$ was statistically significant.

the probe **CyO-Disu**, the *ex vivo* imaging of GSH in isolated organs (heart, liver, spleen, lungs, and kidneys) was performed, which revealed that the fluorescence in Ch1 gathered not only in the liver but also in the lungs, most probably induced by the spread of the hepatoma cells (Fig. 5d). These results demonstrated that the fluorescence imaging in Ch1 of probe **CyO-Disu** could help trace the metastatic position of hepatoma cells. Following this, the average ratio intensities were calculated using the pulmonary metastatic HCC mice image shown in Fig. 5c and are showcased in Fig. 5e. The decrease trend of the mean ratio intensities from 35 to 49 days indicated the decrease of the GSH level with the development of the metastatic hepatoma. Furthermore, the mean ratio intensity values of relevant organs (heart, liver, spleen, lungs, and kidneys) in Fig. 5d again confirmed the data in Fig. 5f. All these results demonstrated that the probe **CyO-Disu** could sensitively detect the GSH level, trace the hepatoma cells metastasis and distinguish the stage of liver cancer (M0, cancer cells in liver or M1, cancer cells in other organs), which might promote the clinical application of the fluorescent probe in the diagnosis and treatment at the advanced stage of HCC.

4. Conclusions

Early diagnosis and subsequent treatment require reliable disease biomarkers. In this work, we have successfully designed and synthesized a ratiometric NIR fluorescent probe **CyO-Disu** for the bioimaging of GSH concentration fluctuations in different stages of HCC. **CyO-Disu** features three key moieties: a fluorophore of NIR heptamethine ketone cyanine, a fluorescence modulator bis(2-hydroxyethyl) disulfide, and a liver-targeting unit D-galactose. Leveraging the intracellular biochemical thiol–disulfide exchange reaction, **CyO-Disu** can respond to GSH selectively and sensitively in several minutes without inference from other biomolecules. The probe **CyO-Disu** has been demonstrated to be profitable in detecting the GSH generation in live RH-35, BRL 3A, SMMC-7721, and HL-7702 cells, as well as the endogenous GSH concentration changes in living RH-35. With D-galactose as hepatocytes targeting unit, the probe **CyO-Disu** can image and evaluate GSH level fluctuations in the orthotopic HCC and pulmonary metastatic hepatoma mice models. The experimental results reveal that the GSH level varies at different stages of HCC, which indicated the potential of employing GSH as a biomarker for the evaluation of HCC development and further therapy. Finally, we envision that the developed probe **CyO-Disu** can be utilized to aid the diagnosis of HCC at an early stage and gain improved treatment.

Conflicts of interest

There are no conflicts to declare.

Acknowledgements

This work was supported by the National Natural Science Foundation of China (No. 21904030, 22264013, 82202222 and 22204037), the Hainan Province Science and Technology Special Fund (Grants ZDYF2022SHFZ288), the Hainan High-Level Talents Project (Grants 820RC654), the Nanhai Young-Talent Program of Hainan (20202018), Hainan Province Clinical Medical Center (2021), the Natural Science Research Talent Project of Hainan Medical University (Grant JBGS202101), Guangzhou Fundamentals and applied fundamentals project (Grant 2023A04J0573), and the Project for Functional Materials and Molecular Imaging Science Innovation Group of Hainan Medical University.

References

1 H. Nakamura, K. Nakamura and J. Yodoi, *Annu. Rev. Immunol.*, 1997, **15**, 351–369.
2 B. Uttara, A. V. Singh, P. Zamboni and R. T. Mahajan, *Curr. Neuropharmacol.*, 2009, **7**, 65–74.
3 K. Oettl and R. E. Stauber, *Br. J. Pharmacol.*, 2007, **151**, 580–590.
4 E. H. Sarsour, M. G. Kumar, L. Chaudhuri, A. L. Kalen and P. C. Goswami, *Antioxid. Redox Signaling*, 2009, **11**, 2985–3011.
5 Y. M. Go and D. P. Jones, *Crit. Rev. Biochem. Mol. Biol.*, 2013, **48**, 173–191.
6 R. L. Siegel, K. D. Miller, H. E. Fuchs and A. Jemal, *Ca-Cancer J. Clin.*, 2022, **72**, 7–33.
7 I. Rahman, A. Kode and S. K. Biswas, *Nat. Protoc.*, 2006, **1**, 3159–3165.
8 E. Camera and M. Picardo, *J. Chromatogr. B: Anal. Technol. Biomed. Life Sci.*, 2002, **781**, 181–206.
9 L. He, L. He, S. Xu, T. Ren, X. Zhang, Z. Qin, X. Zhang and L. Yuan, *Angew. Chem., Int. Ed.*, 2022, **61**, e202211409.
10 Z. Mao, J. Xiong, P. Wang, J. An, F. Zhang, Z. Liu and J. Seung Kim, *Coord. Chem. Rev.*, 2022, **454**, 214356.
11 X. Wu, R. Wang, N. Kwon, H. Ma and J. Yoon, *Chem. Soc. Rev.*, 2022, **51**, 450–463.
12 X. Hu, H. Gan, F. Meng, H. Han, D. Shi, S. Zhang, L. Zou, X. He and T. D. James, *Front. Chem. Sci. Eng.*, 2022, **16**, 1425–1437.
13 J. Wang, F. Huo, Y. Zhang and C. Yin, *Chin. Chem. Lett.*, 2022, 107818.
14 T. Ren, Z. Wang, Z. Xiang, P. Lu, H. Lai, L. Yuan, X. Zhang and W. Tan, *Angew. Chem., Int. Ed.*, 2021, **60**, 800–805.
15 X. Song, R. Wang, J. Gao, X. Han, J. Jin, C. Lv and F. Yu, *Chin. Chem. Lett.*, 2022, **33**, 1567–1571.
16 X. Tian, L. K. Kumawat, S. D. Bull, R. B. P. Elmes, L. Wu and T. D. James, *Tetrahedron*, 2021, **82**, 131890.
17 N. Kwon, C. S. Lim, D. Lee, G. Ko, J. Ha, M. Cho, K. M. K. Swamy, E.-Y. Lee, D. J. Lee, S.-J. Nam, X. Zhou, H. M. Kim and J. Yoon, *Chem. Commun.*, 2022, **58**, 3633–3636.
18 Y. Zou, M. Li, Y. Xing, T. Duan, X. Zhou and F. Yu, *ACS Sens.*, 2020, **5**, 242–249.
19 Y. Yang, K. Zhou, M. Ma, H. Liu, M. Jin, C. Yin, S. Wang and J. Zhang, *Chem. Eng. J.*, 2023, **452**, 139020.

20 H. S. Jung, X. Chen, J. S. Kim and J. Yoon, *Chem. Soc. Rev.*, 2013, **42**, 6019–6031.
21 Y. Yang, T. Zhou, M. Jin, K. Zhou, D. Liu, X. Li, F. Huo, W. Li and C. Yin, *J. Am. Chem. Soc.*, 2020, **142**, 1614–1620.
22 X. Han, X. Song, F. Yu and L. Chen, *Chem. Sci.*, 2017, **8**, 6991–7002.
23 S. Bonengel and A. Bernkop-Schnurch, *J. Controlled Release*, 2014, **195**, 120–129.
24 G. Wu, Y. Fang, S. Yang, J. R. Lupton and N. D. Turner, *J. Nutr.*, 2004, **134**, 489–492.
25 H. Refsum, A. D. Smith, P. M. Ueland, E. Nexo, R. Clarke, J. McPartlin, C. Johnston, F. Engbaek, J. Schneede, C. McPartlin and J. M. Scott, *Clin. Chem.*, 2004, **50**, 3–32.
26 J. Messens and J. F. Collet, *Antioxid. Redox Signaling*, 2013, **18**, 1594–1596.
27 C. S. Lim, G. Masanta, H. J. Kim, J. H. Han, H. M. Kim and B. R. Cho, *J. Am. Chem. Soc.*, 2011, **133**, 11132–11135.
28 M. H. Lee, J. H. Han, P. S. Kwon, S. Bhuniya, J. Y. Kim, J. L. Sessler, C. Kang and J. S. Kim, *J. Am. Chem. Soc.*, 2012, **134**, 1316–1322.
29 M. H. Lee, H. M. Jeon, J. H. Han, N. Park, C. Kang, J. L. Sesser and J. S. Kim, *J. Am. Chem. Soc.*, 2014, **136**, 8430–8437.
30 S. Wang, W. Ren, J. Hou, M. Won, J. An, X. Chen, J. Shu and J. S. Kim, *Chem. Soc. Rev.*, 2021, **50**, 8887–8902.
31 L. Wu, J. Liu, X. Tian, R. R. Groleau, S. D. Bull, P. Li, B. Tang and T. D. James, *Chem. Sci.*, 2021, **12**, 3921–3928.
32 Q. Wu, Q. Zhou, W. Li, T. Ren, X. Zhang and L. Yuan, *ACS Sens.*, 2022, **7**, 3829–3837.
33 S. Zuo, G. Jiang, Y. Zheng, X. Zhang, Z. Qin, L. Chen, T. Ren, X. Zhang and L. Yuan, *Anal. Chem.*, 2023, **95**, 898–906.
34 T. Ma, F. Huo, J. Chao, J. Li and C. Yin, *Sens. Actuators, B*, 2020, **320**, 128044.
35 J. Yin, Y. Kwon, D. Kim, D. Lee, G. Kim, Y. Hu, J. H. Ryu and J. Yoon, *Nat. Protoc.*, 2015, **10**, 1742–1754.
36 H. S. Jung, T. Pradhan, J. H. Han, K. J. Heo, J. H. Lee, C. Kang and J. S. Kim, *Biomaterials*, 2012, **33**, 8495–8502.
37 X. Fan, W. Yang, T. Ren, S. Xu, X. Gong, X. Zhang and L. Yuan, *Anal. Chem.*, 2022, **94**, 1474–1481.
38 J. Navarro, E. Obrador, J. Carretero, I. Petschen, J. Avino, P. Perez and J. M. Estrela, *Free Radical. Biol. Med.*, 1999, **26**, 410–418.
39 G. I. Giles, M. J. Nasim, W. Ali and C. Jacob, *Antioxidants*, 2017, **6**, 38.
40 E. E. Graves, R. Weissleder and V. Ntziachristos, *Curr. Mol. Med.*, 2004, **4**, 419–430.
41 S. Zhang, Z. Zeng, Z. Tang, J. Sun, J. Cheng, R. Liu, P. Wang and B. Zhang, *Hepatol. Int.*, 2008, **2**, 237–243.
42 J. Fang, H. Zhou, C. Zhang, L. Shang, L. Zhang, J. Xu, L. Zheng, Y. Yuan, R. Guo, W. H. Jia, J. Yun, M. Chen, Y. Zhang and S. Zhuang, *Hepatology*, 2015, **62**, 452–465.
43 S. Xu, W. Pan, T. Ren, S. Huan, L. Yuan and X. Zhang, *Chin. J. Chem.*, 2022, **40**, 1073–1082.

